ORIGINAL PAPER

Ion conduction in chitosan-starch blend based polymer electrolyte with ammonium thiocyanate as charge provider

A. S. Mohamed[1] · M. F. Shukur[2] · M. F. Z. Kadir[3] · Y. M. Yusof[1]

Abstract

The global issue of environmental pollution has become the motivation for researchers to develop natural based products. Researchers start to substitute synthetic polymers with natural polymers as host and ammonium salts instead of lithium salts for electrolyte application due to biodegradable, safer to handle and low in cost. In this work, a green polymer electrolyte system is prepared by blending 80 wt.% starch and 20 wt.% chitosan with ammonium thiocyanate (NH_4SCN) as dopant salt. The highest room temperature conductivity of $(1.30 \pm 0.34) \times 10^{-4} \, S \, cm^{-1}$ is obtained when the starch–chitosan blend is doped with 30 wt.% NH_4SCN electrolyte which is found to obey Arrhenius rule. The deconvolution of Fourier transform infrared (FTIR) analysis has proved the molecular interaction between starch, chitosan and NH_4SCN. The number density (n), mobility (μ) and diffusion coefficient (D) of ions are found to be affected by NH_4SCN concentration. This result is further supported by the XRD sample with 30 wt.% NH_4SCN which exhibited the most amorphous structure with the lowest degree of crystallinity. Conduction mechanism for the highest conducting electrolyte follows correlated barrier hopping (CBH) model.

Introduction

Solid polymer electrolytes (SPEs) field has expanded widely because of its high possibility to be utilized as a separator in energy devices such as supercapacitor, sensors, fuel cell and batteries [1]. SPEs are stable for high-temperature performance and have promising mechanical properties which can overcome the drawbacks of liquid electrolyte including leaking, flammability and toxicity [2]. Biopolymer is chosen as polymer host in electrolyte because it is a good candidate due to biodegradability, renewability and biocompatibility [3]. Biopolymers such as starch [4], cellulose [5], chitosan [6] and dextrin [7] have been studied for potential application as SPE.

Starch contains largest carbohydrate originated from food including rice, potatoes, wheat and corn [8]. Starch consists of the combination of polysaccharides, which are amylose and amylopectin [9]. Two main chains which are α-(1, 4)-linked D-glucose; as a minor component with linear group can be assumed a helical shape and can form inclusion compounds, combined with α-(1, 6)-glycosidic linkage; which contains packing arrangement of double helices with high molecular weight. These structures cause the low mobility of the polymer chains hence increase the crystalline phase to form branches in the polymers [10, 11]. Chitosan is very useful due to their unique characteristics such as highly amorphous and can form mechanically strong film. It is widely applied in food industry and biomedical sectors [12–14]. There are two functional groups in chitosan; amine and hydroxyl that contribute to the complexation of polymer blend and salt [15, 16].

Polymer blend offers high amorphous region compared to a single polymer [17, 18], therefore polymer blend has been widely used to improve the properties of SPEs [19, 20]. Starch and chitosan are found to be compatible to serve as polymer blend host due to high mechanical strength with low degree of crystallinity [21, 22]. Previous studies prove ammonium salt is a good ion provider to polymer electrolytes [23, 24]. Conductivity of phthaloyl chitosan (Phch) doped with

✉ Y. M. Yusof
  yuhanees@unikl.edu.my

1 Chemical Engineering Section, Universiti Kuala Lumpur, Malaysian Institute of Chemical & Bioengineering Technology (UniKL MICET), Alor Gajah, 78000 Malacca, Malaysia

2 Fundamental and Applied Sciences Department, Universiti Teknologi PETRONAS, 32610 Seri Iskandar, Perak, Malaysia

3 Centre for Foundation Studies in Science, University of Malaya, 50603 Kuala Lumpur, Malaysia

NH_4SCN has been reported by Aziz et al. [25] to reach maximum conductivity of $(2.42 \pm 0.01) \times 10^{-5}$ S cm^{-1} at room temperature with 30 wt.% salt. In other previous work a single polymer of starch doped with NH_4SCN with 50:50 ratio has reported the ionic conductivity has reached to 7.47×10^{-7} S cm^{-1} at room temperature [26]. In this paper, the structural and electrical behaviour of chitosan-starch polymer blend doped with NH_4SCN are investigated. The transport properties are also analysed based on the deconvolution of FTIR spectra.

Experimental

Electrolyte preparation

Corn starch (Brown & Polson) and chitosan (Sigma-Aldrich) with viscosity of 800–2000 cP (MW = 310,000–375,000) and degree of deacetylation >75% were used to prepare the polymer host. Ammonium thiocyanate (NH_4SCN) was purchased from HmbG while acetic acid was purchased from SYSTERM. Solution cast technique was used to prepare the polymer electrolytes. Starch solution was prepared by dissolving 0.8 g corn starch in 100 ml of 1% acetic acid at 80 °C for 20 min. After the solution was cooled to room temperature, 0.20 g of chitosan was added. Different concentrations of NH_4SCN was added to the 4:1 starch-chitosan blend solution and stirred until a homogeneous solution was obtained. All solutions were cast on plastic Petri dishes and left to dry at room temperature. The dry films were kept in a glass desiccator filled with silica gel desiccants for further drying. All the electrolyte compositions are tabulated in Table 1.

Electrolytes characterization

Fourier transform infrared (FTIR) spectroscopy was performed using Spotlight 400 Perkin-Elmer spectrometer in the transmission mode resolution of 4 cm^{-1} from 450 to 4000 cm^{-1}. The FTIR spectra were deconvoluted using nonlinear fitting software due to the overlapping peaks. In order to deconvolute the FTIR spectra, baseline correction and curve fitting were applied using Lorentzian-Gaussian method to

Table 1   Designation of electrolytes

Chitosan-Starch: NH$_4$SCN(wt.%)	Designation
100:0	S0
90:10	S1
80:20	S2
70:30	S3
60:40	S4

extract the exact and overlapping peaks. X-ray diffraction (XRD) analysis was done using Siemens D5000 X-ray diffractometer (1.5406 Å). The angle 2θ was varied from 5° to 80°. Deconvolution of XRD was done to determine the degree of crystallinity (X_c) electrolytes using the following:

$$X_c = \frac{A_c}{A_T} \times 100 \qquad (1)$$

where A_c is the total area of crystalline peaks and A_T is the total area of crystalline and amorphous peaks. Impedance analysis was carried out using HIOKI 3532–50 LCR HiTESTER from 50 Hz to 5 MHz at various temperatures. The electrolytes were placed between two stainless steel electrodes of a conductivity case. The conductivity is calculated by using:

$$\sigma = \frac{t}{A \, R_B} \qquad (2)$$

where t is the thickness of electrolytes, R_B is the bulk resistance obtained from the Cole-Cole plots and A is the electrode-electrolyte contact surface area.

Results and discussion

Conductivity analysis

Figure 1 shows the ionic conductivities of electrolytes as a function of NH_4SCN concentration. The ionic conductivity directly depends on the charge carrier concentration. Therefore, when the charge concentration is changed by doping the polymer with different concentrations of salt, the conductivity is also expected to change [21]. When 10 wt.% of NH_4SCN is added to the electrolyte, the conductivity of pure starch-chitosan film increases from 4.05×10^{-10} S cm^{-1} to 9.03×10^{-9} S cm^{-1}. The conductivity is further increased to 7.75×10^{-6} S cm^{-1} with the addition of 20 wt.% NH_4SCN salt. This phenomena is attributed to the increased in the number of charge carriers [27]. The highest ionic conductivity is obtained when 30 wt.% of NH_4SCN is added to the
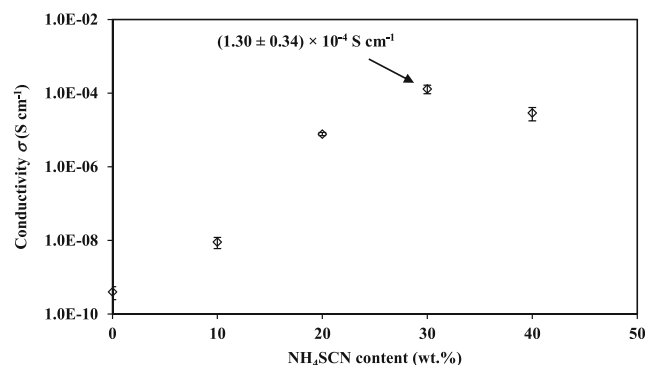

Fig. 1 Effect of NH_4SCN content on conductivity of electrolyte at room temperature

electrolyte. The increment can be related to the increased in the number of mobile charge carriers and the decrease in crystallinity which will be proven in XRD result [28].

Chitosan doped with NH$_4$SCN was reported to obtain the highest conductivity of $(2.42 \pm 0.01) \times 10^{-5}$ S cm^{-1} at room temperature [25]. Hence, the higher ionic conductivity obtained in this work proves that the blending method is a promising technique to enhance the conductivity of the electrolyte. At the concentration of NH$_4$SCN above 30 wt.%, the conductivity decreases to 2.91×10^{-5} S cm^{-1} because the distance between dissociated ions become too close, therefore they are able to recombine and form neutral ion pairs that do not contribute towards conductivity. As the consequence, the ion triplets, ion pairs and ion aggregation will drop the conductivity due to the decrease in number density and mobility of ion [29].

The conductivity behaviour of the highest conducting electrolyte in starch-chitosan doped with NH$_4$SCN system at elevated temperatures is shown in Fig. 2. The Arrhenius equation (Eq. 3) can be used due to the temperature relation with the conductivity.

$$\sigma = \sigma_o \exp\frac{E_a}{k\,T} \tag{3}$$

where σ_o is the pre-exponential factor, E_a is the activation energy, k is the Boltzmann constant and T is the absolute temperature. The activation energy value obtained for S3 electrolyte is 0.264 eV which calculated using the slop of the plot and Arrhenius equation. The ionic conductivity of the electrolyte is increased with the increasing temperature, confirming the Arrhenius behaviour where the regression value is close to unity, $R^2 \sim 1$. Low E_a shows that the ions require low energy to be free from one coordinating site to move to another coordinating sites [27]. The report by Buraidah et al. [27] for chitosan acetate system shows an E_a value of 0.46 eV with the addition of 40 wt.% NH$_4$I. Zulkefli et al. [30] reported that starch system doped with 30 wt.% of NH$_4$SCN resulted the minimum E_a value at 0.28 eV.

The VTF and Arrhenius behaviours of ionic conduction have been widely reported in polymer electrolytes [31, 32]. In amorphous region, ionic conduction is assisted by polymer
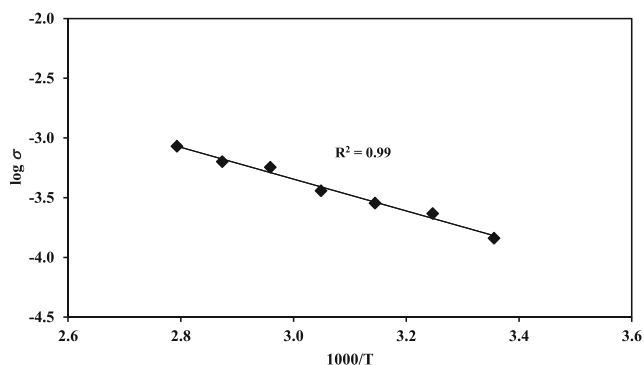
Fig. 2 The ionic conductivity behaviour at elevated temperatures

segmental motion above the glass transition temperature (T_g), which describes the VTF type behaviour. In crystalline region, an Arrhenius type ionic motion is often observed [33]. Most polymers for polymer electrolytes are semi-crystalline materials. The existence of crystalline region below melting point (T_m) prevents the segmental motion in the host polymer [34]. Above the melting temperature, the crystalline regions are completely absent, hence significant contribution of segmental motion to the ionic conduction is expected [35]. From a report by Shukur et al. [36], the T_g of pure starch-chitosan is 82.33 °C. It is known that T_m is higher than the T_g [37]. Thus, it is expected that the T_m value of starch-chitosan blend is higher than 82.33 °C. In this work, the conductivity of S3 is studied in the temperature range of 298 K (25 °C) to 358 K (85 °C). Since the temperature range is below the T_m of starch-chitosan, the conductivity-temperature relation for the present electrolytes obey Arrhenius rule. This result is comparable with previous study where CMC doped with NH$_4$SCN electrolyte system reported by Noor et al., obey Arrhenius rule [38]. The electrolyte system of PVA-amino acid proline cooperated with NH$_4$SCN reported by Hemalatha et al. [23] and PVA-PAN doped with NH$_4$SCN reported by Premalatha et al. [39] were also showed these two systems obey the Arrhenius behaviour.

FTIR analysis

The complexation between polymer blend and salt and the identification of functional groups can be observed by FTIR spectroscopy. Figure 3(a) shows the FTIR spectra for broad hydroxyl (OH) band region between 2800 to 3800 cm^{-1} for selected electrolytes. The hydroxyl band region for this starch-chitosan blend film, S0 is located at 3292 cm^{-1} which is comparable with previous study reported by Yusof et al. [21]. The change in peak position, intensity and shape of S0 spectrum is due to the interaction between starch and chitosan in this region. The position of hydroxyl peak in S0 shifts to lower wavenumber from 3292 cm^{-1} to 3284 cm^{-1} when 10 wt.% of salt is added to the polymer blend. This trend is similar as reported by Shukur et al. [36]. The addition of 5 and 10 wt.% of ammonium chloride, NH$_4$Cl in their work has shifted the wavenumber of polymer blend from 3288 cm^{-1} to lower wavenumber of 3284 cm^{-1} and 3278 cm^{-1}, respectively. In the spectrum of pure NH$_4$SCN salt, two peaks appear in the hydroxyl band region. These two peaks appear at 3108 and 3025 cm^{-1}, corresponding to the asymmetry vibration υ_{as} (NH$_4^+$) and symmetry vibration υ_s (NH$_4^+$) modes respectively. These two peaks are similar as reported by Kadir and Hamsan in dextran-chitosan-NH$_4$SCN system where asymmetry vibration υ_{as} (NH$_4^+$) and symmetry vibration υ_s (NH$_4^+$) appear at 3099 cm^{-1} and 3014 cm^{-1}, respectively [40]. Figure 3(b) displays the saccharide band region between 950 to 1050 cm^{-1} which often assigned as the bending mode

Fig. 3 FTIR spectra for (a) hydroxyl band region and (b) saccharide band region
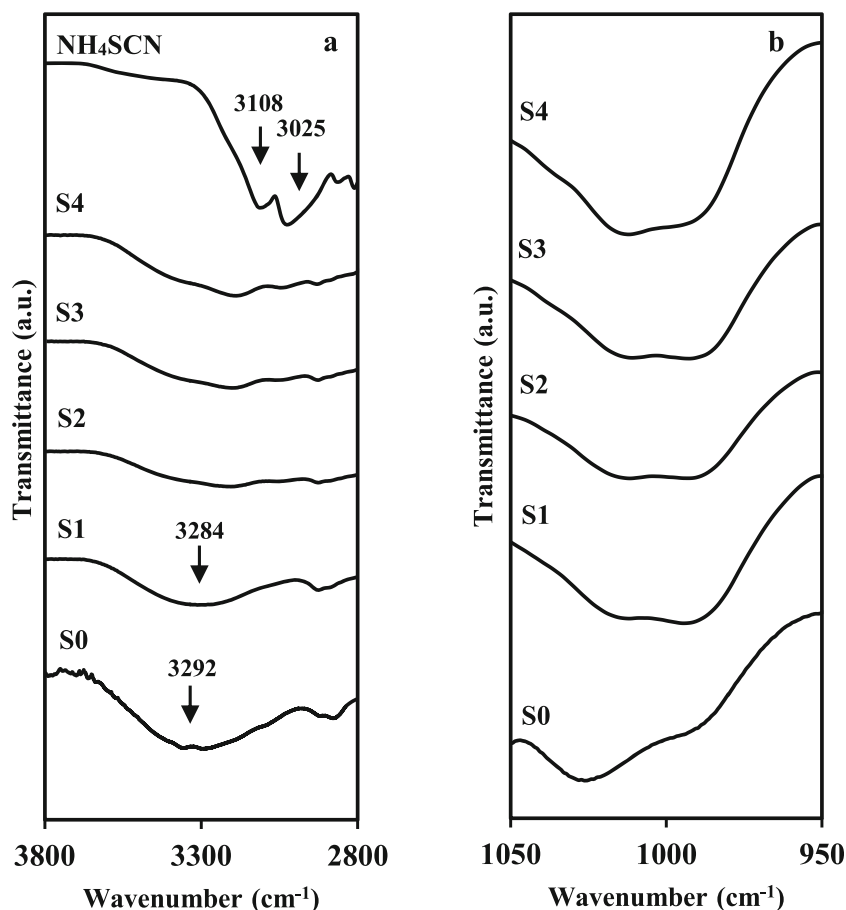
of C-O-H bonds and C-O stretching vibration modes [8]. The band locations can be compared to the report by Yusof et al. [41]. In their report, the C-O-H band was observed at 1007 cm^{-1} for starch-chitosan polymer blend while the stretching vibration of C-O in the saccharide group is shown at 990 cm^{-1} [41]. This phenomenon is an evidence of the interaction between nitrogen atoms of the polymer matrix with the cations (H$^+$) [6].

The peaks in the range of 3020 to 3560 cm^{-1} are fitted and deconvoluted as showed in Fig. 4. Due to the possibility of overlapping bands OH band with υ_{as} (NH$_4^+$) and υ_s (NH$_4^+$), deconvolution technique has been carried out for selected electrolytes. From the deconvolution pattern, it shows that the hydroxyl band is more intense for the samples with higher salt contents. On the addition of 20 and 30 wt.% of NH$_4$SCN, the hydroxyl band of S2 and S3 are shifted to higher wavenumbers which are 3359 cm^{-1} and 3379 cm^{-1}, respectively. As more salt is added to the electrolytes, this leads to higher ionic conductivity due to the increment of charge carriers. The hydroxyl band in S4 is then shifted back to lower wavenumber at 3365 cm^{-1} for the addition of 40 wt.% NH$_4$SCN. Due to excess salt, the ions tend to reassociate and lead to the decrement of ionic conductivity. The FTIR results presented are comparable with the report by Kadir

et al. [42] when the hydrogen band region in their chitosan-ammonium nitrate (NH$_4$NO$_3$) system has shifted to lower wavenumber with the addition of 10 and 30 wt.% of NH$_4$NO$_3$.

The υ_{as} (NH$_4^+$) peak in S2 has shifted from 3186 cm^{-1} to 3197 cm^{-1} in S3 corresponded to the change in salt content and the peaks become closer to each other [4]. The interaction of cations, H$^+$ with oxygen atom of hydroxyl group leading to the increment of ionic conductivity at room temperature [40]. The addition of 40 wt.% salt in S4 cause the υ_{as} (NH$_4^+$) shifted to lower wavenumber at 3190 cm^{-1} due to the formation of ions aggregates which reduce the interaction. The υ_s (NH$_4^+$) peak of S2 at 3079 cm^{-1} shifted to lower wavenumber of 3040 cm^{-1} and 3035 cm^{-1} when 30 wt.% and 40 wt.% of salt is added to electrolytes. The appearance of υ_{as} (NH$_4^+$) and υ_s (NH$_4^+$) modes justify the occurrence of ions reassociation when more than 30 wt.% NH$_4$SCN is added to electrolyte hence to lead the decrement of the ionic conductivity.

Figure 5 shows the deconvolution that has been done to further analyse the FTIR spectra for saccharide band region from 972 to 1042 cm^{-1}. The band for polymer blend, S0 is located at 1026 cm^{-1} and 989 cm^{-1} which assigned as C-O-H bond and C-O in saccharide respectively. The C-O-H peak of S0 has shifted to 1012 cm^{-1} while C-O peak shifted to 990 cm^{-1} when 10 wt.% of salt is added to

**Fig. 4** Deconvoluted of FTIR spectrum for 3020–3560 cm^{-1} region
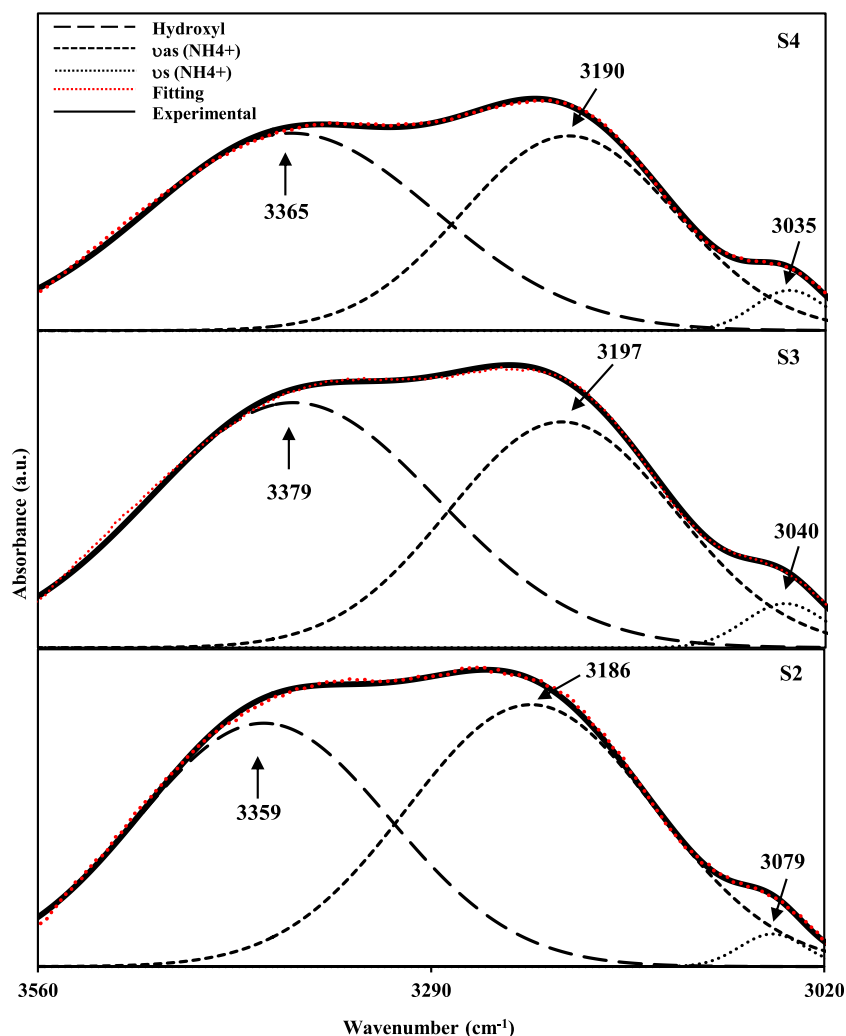
the electrolyte. When the salt concentration is increased, the peaks are found to be shifted to higher wavenumber from 1012 and 990 cm^{-1} for S1 to 1014 and 992 cm^{-1} for S2 and 1018 and 994 cm^{-1} for S3. These changes prove that when the polymer blend is doped with NH$_4$SCN, there are interactions between starch-chitosan with NH$_4$SCN at C-O-H and C-O band regions [3]. However, the peaks decrease from 1018 and 994 cm^{-1} in S3 to 1015 and 990 cm^{-1} in S4 when 40 wt.% of NH$_4$SCN is added to the system. This could be attributed to the overloaded of NH$_4$SCN hence reduce the interaction between polymer host and salt [6]. Reduction of the interaction contributes the recrystallization of the salt in S4 which leads to the decreased in conductivity [43]. These bands are sensitive to crystallinity where the changes in shapes and intensity at these regions can be directed to the transition from amorphous to semi crystalline structure [44]. This result is further confirming the trend of ionic conductivity at room temperature of this polymer electrolyte system.

Transport properties

The dissociation of ions and the transport parameters, which are number density of charge carriers, n, mobility of charge carriers, μ and diffusion coefficient of charge carrier, D can be determined from FTIR deconvolution method at free ions region. The result from transport parameters are correlated to the ionic conductivity of starch-chitosan doped with NH$_4$SCN salt.

Figure 6 shows the intense peak of SCN$^-$ in salted system of starch-chitosan doped with NH$_4$SCN. The intensity of the peak is increased with the increment NH$_4$SCN salt in the electrolytes. Deconvolution technique is used to study the effect of ions dissociation in the starch-chitosan doped with NH$_4$SCN system. Woo et al. [45] reported two alternative reactive sites which come from SCN$^-$ as an ambient linear anion. These two reactive sites can form N-bonding, S-bonding and bridge complexes of the S and N atom which are C-N stretching, C-S stretching and SCN bending, respectively. Hence, it will lead to the formation of free ions, H$^+$ which contributes to the ionic conductivity. N-bonding requires high absorption

Fig. 5 Deconvoluted of FTIR spectrum for 972–1042 cm^{-1} region
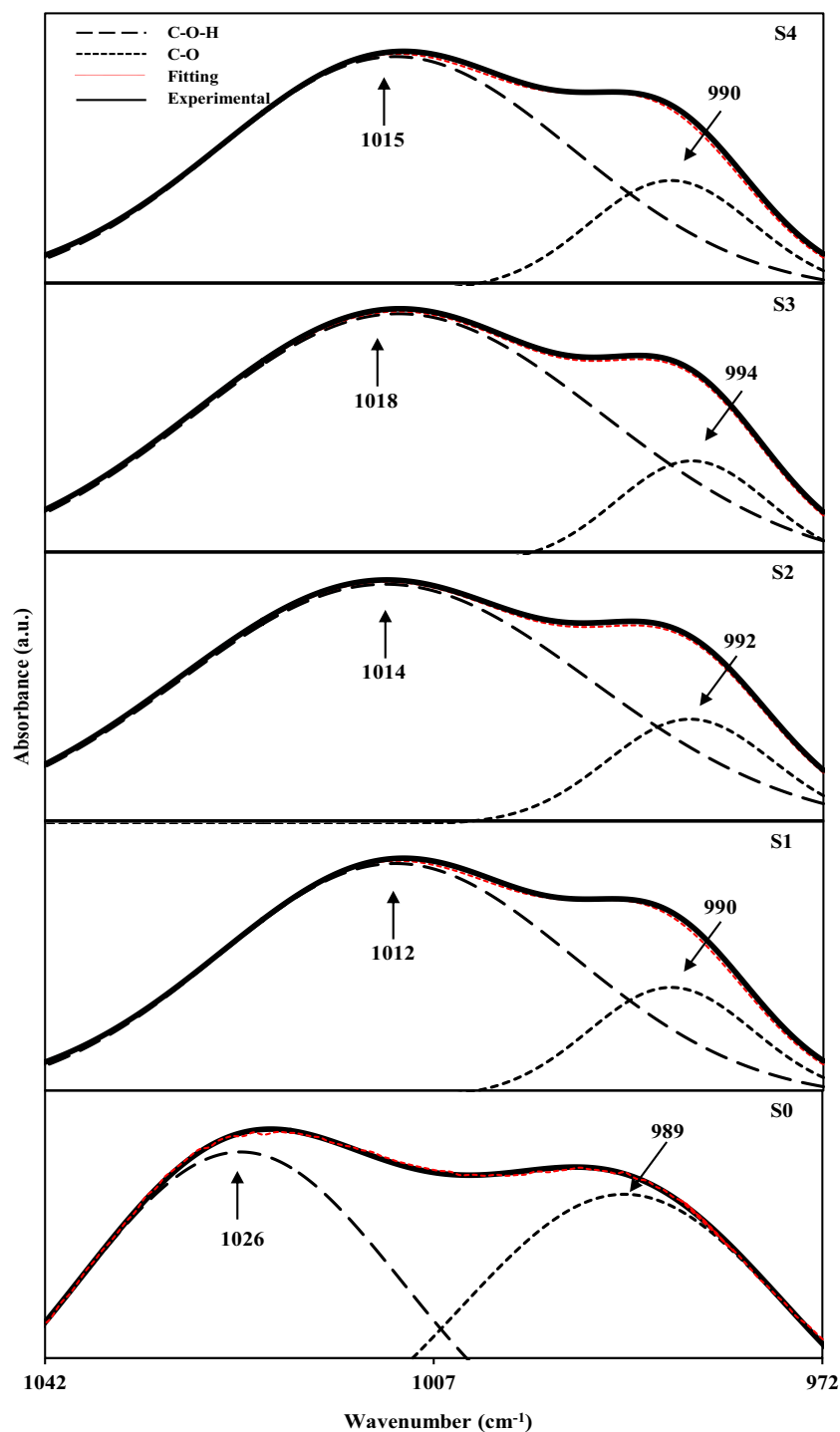
intensity and high sensitivity at C-N stretching in its ionization states [38]. Therefore, the study of SCN$^-$ band region is significance for dissociation of ions in this electrolyte system.

Figure 7 illustrates the deconvolution of SCN$^-$ band region for starch-chitosan doped with NH$_4$SCN at 2010–2100 cm^{-1}. Ramya et al. [46] reported that the peaks at 2072, 2061 and 2047 cm^{-1} represent the formation of ions aggregates, the contact ions (NH$_4^+$ and SCN$^-$) and free

anions (SCN$^-$). Rahman et al. [47] have reported this broad peak consists of three narrowed peaks located at 2070, 2062 and 2038 cm^{-1} while Woo et al. [45] reported at 2074, 2062 and 2038 cm^{-1}. The percentage of ionic species, free ion, contact ions and ions aggregates of starch-chitosan doped with NH$_4$SCN system are calculated from the area under the corresponding band by using the following equation:
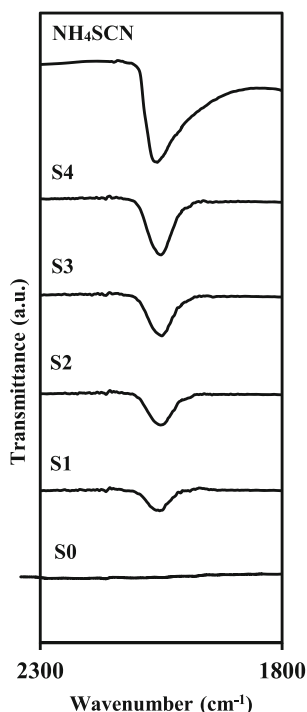
Fig. 6 FTIR spectra for SCN^- stretching

$$Free\ ions\ (\%) = \frac{A_f}{A_f + A_c + A_a} \times 100 \qquad (4)$$

where A_f is the area under the peak respects to the free ions region, A_c is the area under the peak respects to the contact ions region and A_a is the area under the peak respects to the ions aggregates region.

Figure 8 shows the percentage of free ions against the NH$_4$SCN salt concentration. The percentage of free ions is increased with the addition of NH$_4$SCN concentration which leads to the increment of ionic conductivity. Woo et al. reported that the ionic conductivity was improved corresponding to the increment of ions dissociation as well as number of free ions from ammonium salt [45]. As depicted in Fig. 8, the highest percentage of free ions is presented by starch-chitosan electrolyte containing 30 wt.% of salt. Similar observation has been reported by Woo et al. [45] in PCL-NH$_4$SCN system with the highest free ions percentage of 37%. Rahman et al. [47] also reported that their PMMA-ENR-NH$_4$SCN system containing 12 wt.% of salt exhibited the highest free ions of 41%. The transport parameters which are number density of charge carriers, n, mobility of charge carriers, μ and diffusion coefficient of charge carrier, D are obtained using the following equations [46, 48]:

$$n = \left(\frac{M \times N_A}{V_{total}}\right) \times Free\ ions(\%) \qquad (5)$$

$$\mu = \frac{\sigma}{n\ e} \qquad (6)$$

$$D = \frac{\mu\ k\ T}{e} \qquad (7)$$

where M is the number of moles of NH$_4$SCN salt used in each electrolyte, N_A is Avogadro's number, σ is the ionic conductivity, e is the electric charge, K is the Boltzmann constant, T is the absolute temperature and V_{total} is the total volume of the electrolyte.

Table 2 shows the percentages of free ions and value of transport parameters which are n, μ and D. The percentage of free ions is increased with n, following the increment in the concentration of NH$_4$SCN up to 30 wt.%. More ions dissociation occur with the enhancement of NH$_4$SCN concentration hence affect the number density of charge carriers (n) as well as the ionic conductivity [38]. From Table 2, the value of n lies between 2.78×10^{21} cm^{-3} to 4.01×10^{21} cm^{-3}, μ is in between 2.03×10^{-11} cm^2 V^{-1} s^{-1} to 2.02×10^{-7} cm^2 V^{-1} s^{-1}, while the D value is in the range of 5.21×10^{-13} cm^2 s^{-1} to 5.20×10^{-9} cm^2 s^{-1}. Hawzhin et al. [49] reported that the system of PEO-MC doped with NH$_4$I exhibited the highest conductivity value of 7.62×10^{-5} S cm^{-1} which possessed the highest μ and D values of 2.07×10^{-6} cm^2 V^{-1} s^{-1} and 5.42×10^{-8} cm^2 s^{-1}, respectively. Figure 9 shows the plots of transport parameters in this salted system. As can be seen, the plots follow the trend of ionic conductivity. At low concentration of salt, the free ions easily migrate via the coordinating sites which leads to conductivity enhancement [50]. It can be seen that n is increased as the salt concentration increases which also affects the μ and D values. An optimum concentration of salt allows the polymer blend to offer a favourable environment for ions migration with balanced interactions. This result is comparable with a report by M.A. Ramli et al. [51] where the highest conducting electrolyte had the highest values of μ and D. However, μ is dropped when 40 wt.% of salt is added to the electrolyte. This is due to the overcrowding phenomenon as well as the recombination of free ions, hence reduce the ability of ions to mobile and migrate within the polymer host. Therefore, the value of μ as well as D will decrease, following the reduction of ions density. At this concentration, dipole interactions between H$^+$ in the starch-chitosan-NH$_4$SCN system are changed as suggested by the crystallization pattern observed in XRD analysis which will be discussed in XRD section.

XRD analysis

Figure 10 shows XRD patterns for pure NH$_4$SCN salt and selected electrolytes in salted system. It can be seen that S3 shows that the sample is highly amorphous when 30 wt.% NH$_4$SCN is added to the electrolyte compared to S1, S2 and S4. Observation in S4 gives five peaks attributed to the recrystallization of NH$_4$SCN at $2\theta = 21.1°$, $24.1°$, $26.8°$, $28.5°$ and $30.3°$. The crystalline peaks of NH$_4$SCN are comparable with

Fig. 7 Deconvolution of SCN^- band in the region of 2020–2090 cm^{-1} for S1-S4 electrolytes

- – – – – Free ion
- – – – – Contact ion
- – – – – Ion aggregate
- —— Experimental
- ······· Fitting
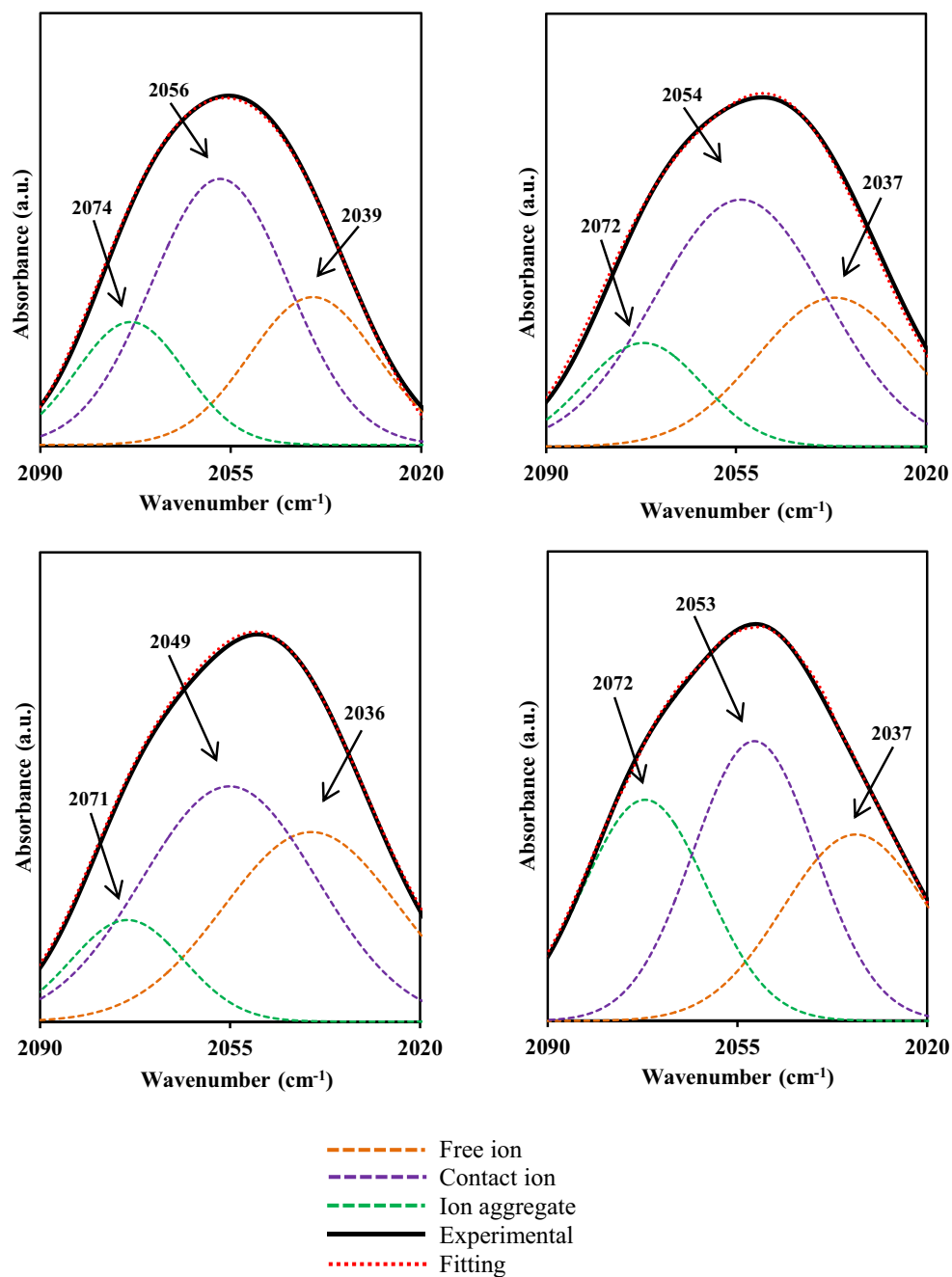
the study reported by Kadir and Hamsan [40]. The intensity of the NH$_4$SCN peaks increases as the salt concentration increases. This is because the polymer host is unable to accommodate the salt which leads to the recombination of the ions and resulted in conductivity decrement [17]. In order to confirm this result, the deconvolution technique is used to extract any possible overlapping peaks of amorphous and crystalline regions. The broad peaks attributed to amorphous region while the sharp and narrow peaks are for crystalline region [52]. The degree of crystallinity can be calculated using (Eq. (1)) and listed in Table 3.

The crystallinity is further analyzed using deconvolution technique as presented in Fig. 11. When NH$_4$SCN is added to the S0 blend, one crystalline peak appears at $2\theta = 32.1°$ which observed as the peak of NH$_4$SCN [53]. Besides, the intensity of the peaks at $2\theta = 13.1°$, $16.9°$ and $23.9°$ in S0 blend decreases in the XRD pattern of S1 at $2\theta = 14.0°$, $17.1°$ and $23.2°$. The intensity of amorphous peaks at $2\theta = 21.3°$ and $40.3°$ for S0 has increased in S1 and located at $2\theta = 21.1°$ and $40.2°$. S1 shows lower degree of crystallinity compared to S0 due to the improvement in the amorphous region. Deconvoluted
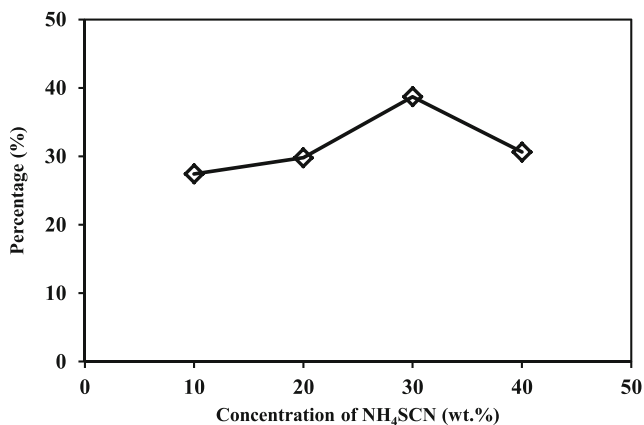
Fig. 8 Percentage of free ions as a function of NH$_4$SCN concentration

XRD patterns of S2 and S3 show the intensity of four crystalline peaks at 2θ = 12.1°, 16.9°, 23.2° and 34.6° for S2, and 2θ = 12.9°, 20.2°, 23.2° and 32.9° for S3 is further decreased. These results can be proven based on the degree of crystallinity of the electrolytes which reduced due to the decreasing of crystalline peaks intensity. The large amorphous region of S3 is supported with the lowest degree of crystallinity compared to other electrolytes. Deconvolution of XRD pattern for S4 electrolyte shows more crystalline peaks attributed to NH$_4$SCN salt. The presence of these peaks proves that the salt has been recrystallized hence drop the number density of ions as well as the ionic conductivity value, as discussed in the transport properties section [40]. The migration of ions is mainly occur in amorphous region due to the polymer segmental motions [54]. Therefore, the values of degree of crystallinity are directly correlated to the ionic conductivity.

Dielectric analysis

The ionic conductivity trend can also be verified by dielectric studies. Dielectric constant characterised the charge stored in a material while dielectric loss characterised the value of energy losses to move ions [34]. The values of ε_r and ε_i are calculated from the equations below:

$$\varepsilon_r = \frac{z_i}{\left(z_r^2 + z_i^2\right) \omega c_o} \qquad (8)$$
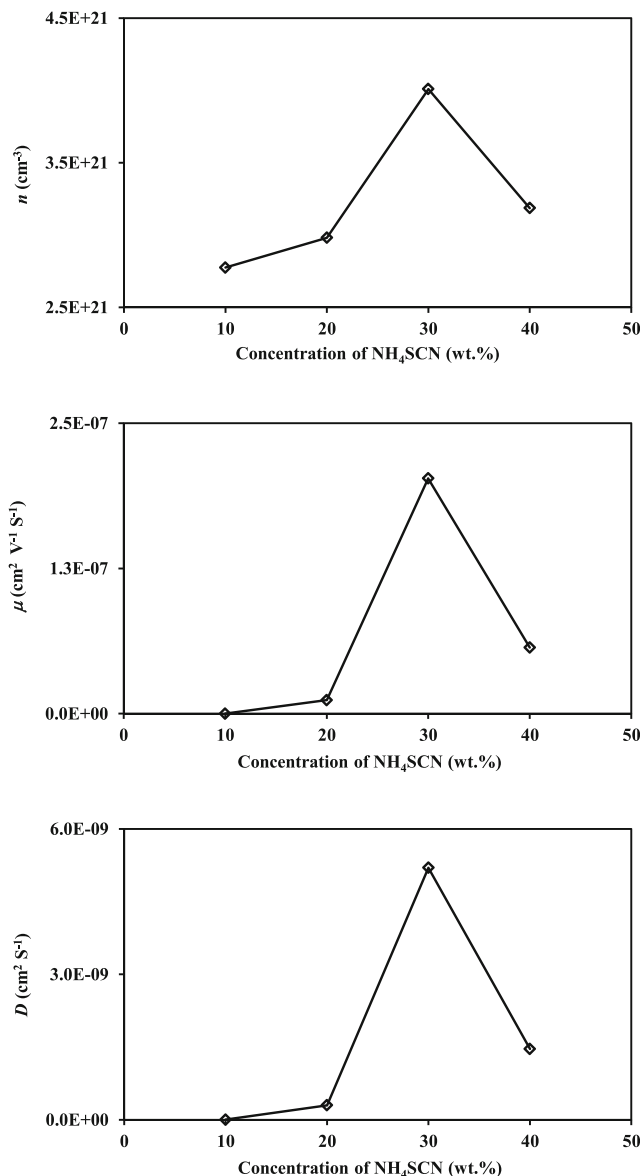

Fig. 9 The transport parameters of n, μ and D for starch-chitosan doped with NH$_4$SCN system

$$\varepsilon_i = \frac{z_r}{\left(z_r^2 + z_i^2\right) \omega c_o} \qquad (9)$$

Table 2 The value of conductivity, percentage of free ions with n, μ and D

Samples	Conductivity, σ (S cm^{-1})	Free ion (%)	Number of density, n (cm^{-3})	Ionic mobility, μ (cm^2 V^{-1} s^{-1})	Diffusion coefficient, D (cm^2 s^{-1})
S1	$(9.03 \pm 0.30) \times 10^{-9}$	27.44	2.78×10^{21}	2.03×10^{-11}	5.21×10^{-13}
S2	$(7.75 \pm 0.39) \times 10^{-6}$	29.79	2.98×10^{21}	1.16×10^{-08}	2.98×10^{-10}
S3	$(1.30 \pm 0.34) \times 10^{-4}$	38.72	4.01×10^{21}	2.02×10^{-07}	5.20×10^{-09}
S4	$(2.91 \pm 0.11) \times 10^{-5}$	30.63	3.19×10^{21}	5.69×10^{-08}	1.46×10^{-09}

Fig. 10 X-ray diffraction patterns
for salted system
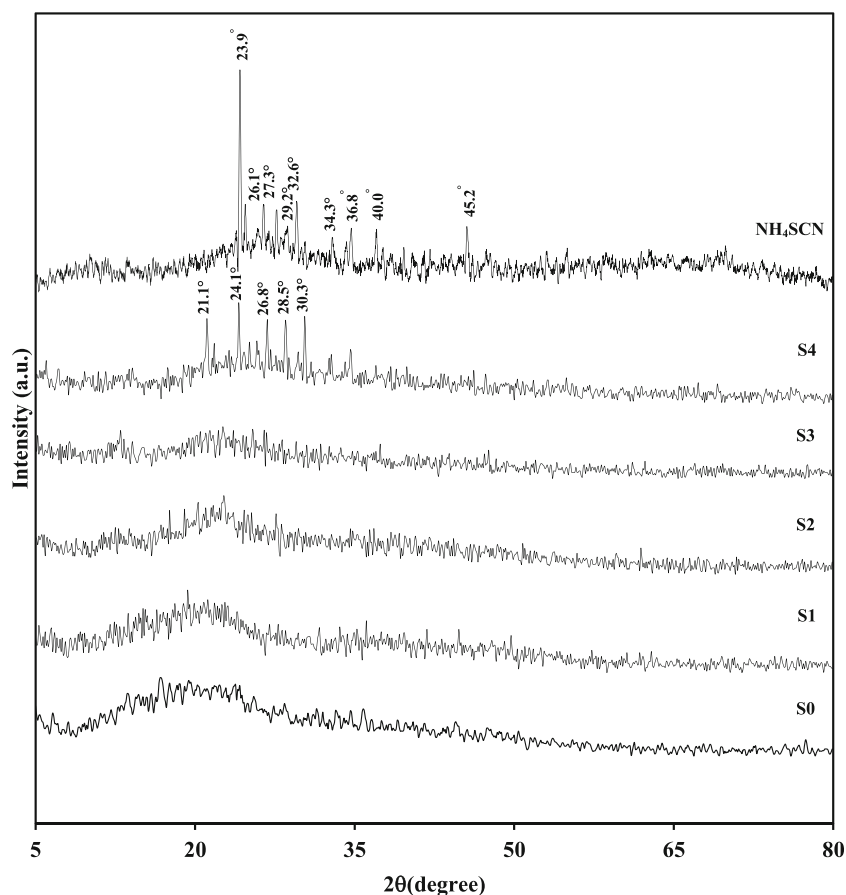
where C_0 is vacuum capacitance, ω is angular frequency, Z_r and Z_i is the real and imaginary parts of impedance, respectively.

Figure 12 (a) and (b) show the dependence of ε_r and ε_i at selected frequencies. It can be noticed that at low frequencies, the values of ε_r and ε_i are higher compared to that of higher frequency. This is because at low frequency, the charges are able to accumulate at the electrolyte-electrode interphases causing the electrode polarization to occur [7]. High frequency causes a fast rate of periodic reversal of the electric field which reduces the dielectric constant [55]. As the amount of NH4SCN increases, the values of ε_r and ε_i are increased hence attributed to the increment of number of charge carriers. However, when the salt content exceeds 40 wt.%, the values of ε_r and ε_i are decreased. At high salt concentration,

reassociation or recombination of ions is favourable thus leading to the decrement of ionic conductivity [56].

Conduction mechanism

Universal Jonscher's Power Law (UPL) can be used to analyse the AC conductivity phenomenon based on equation:

$$\sigma\left(\omega\right) = \sigma_{dc} + A\,\omega^s \tag{10}$$

$$\sigma_{dc} = A\,\omega^s \tag{11}$$

where $\sigma(\omega)$ is the sum of AC and DC conductivity, σ_{dc} frequency independent component, A is temperature dependent parameter and S is the power law exponent with a range from $0 < S < 1$. The AC conductivity can be obtained from dielectric loss, ε_i at every frequency.

$$\sigma_{ac} = \varepsilon_o \varepsilon_i \omega \tag{12}$$
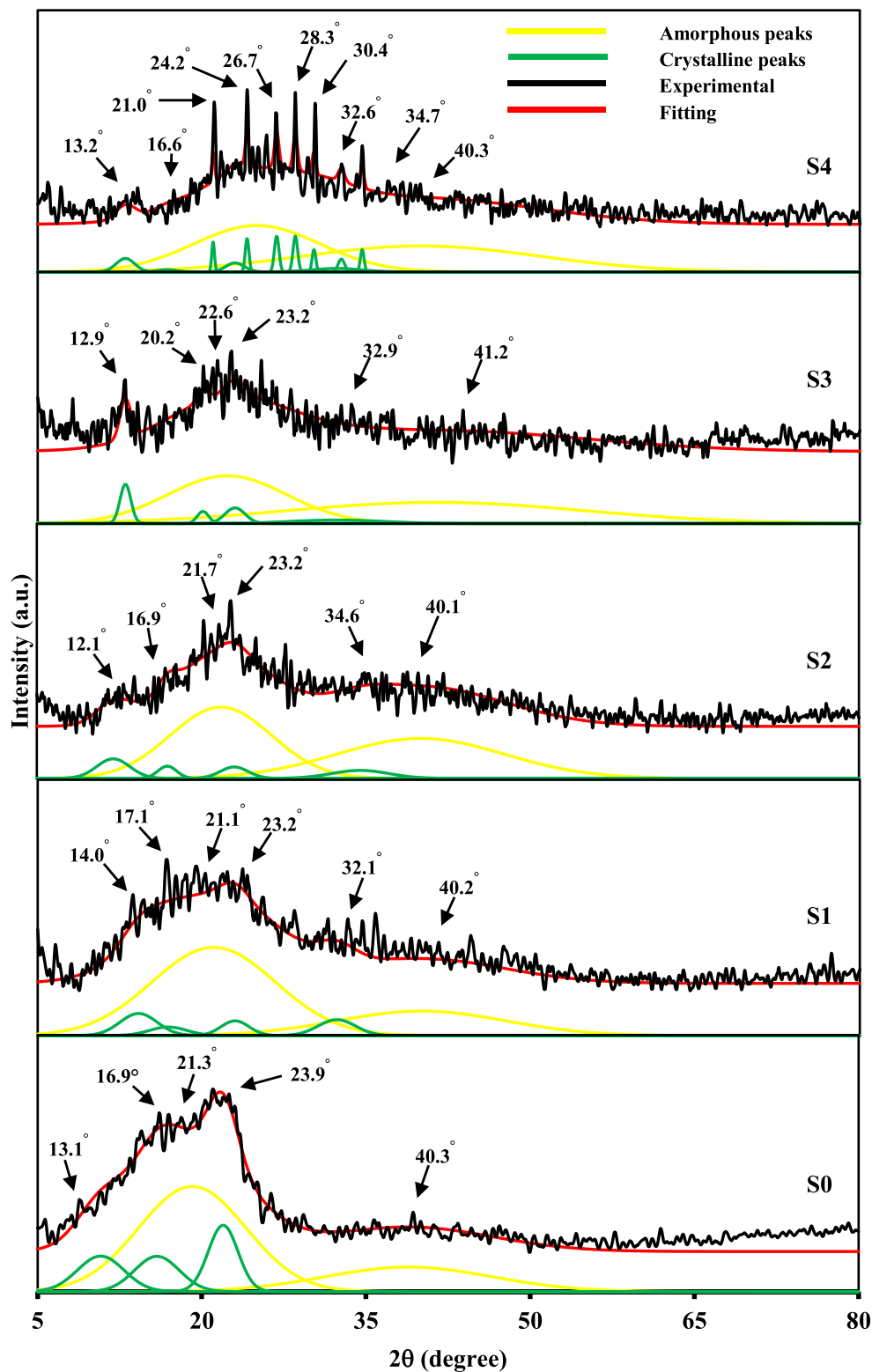
Substituting (Eq. (11)) into (Eq. (12)) and applying logarithm rule, will give

$$\ln\varepsilon_i = \ln\frac{A}{\varepsilon_o} + (S-1)\ln\omega \tag{13}$$

Table 3 Degree of crystalinity of electrolytes

Electrolytes	Degree of crystalinity (X_c)
S1	12.51
S2	9.21
S3	6.98
S4	10.57

Fig. 11 Deconvolution of X-ray diffraction patterns for salted system

In order to show the conduction mechanism behaviour in the system, UPL is used for conduction modelling analysis. Fig. 13 shows the dependence of dielectric loss, ε_i at selected temperatures of the highest conducting electrolyte, S3. The ionic conductivity is found to increase with frequency. The value of s can be found from the slope of
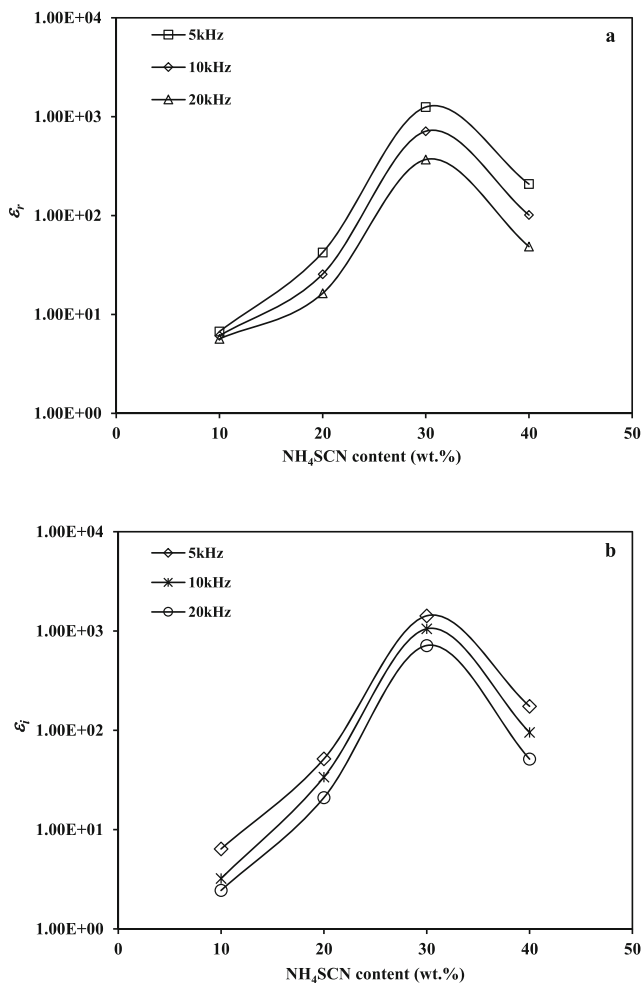
Fig. 12 The dependence of (a) ε_r and (b) ε_i at room temperature for selected frequencies

ln ε_i vs ln ω plot while the plot of exponent s versus temperature is shown in Fig. 14.

Conduction mechanism can be categorized in several behaviours due to the pattern of exponent s values versus temperature. Firstly, value of exponent s is independent of temperature which classified as quantum mechanical tunnelling (QMT) [57], value of exponent s is increased with temperature
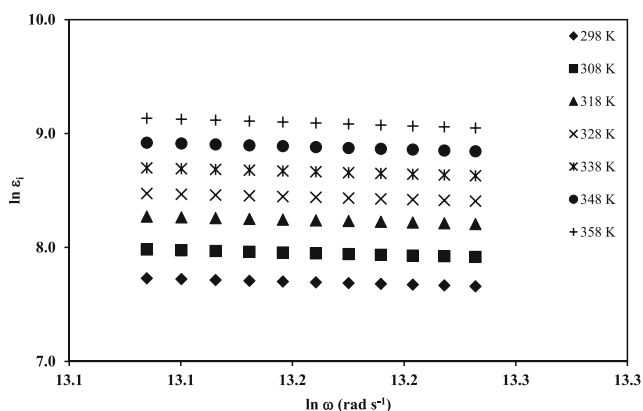

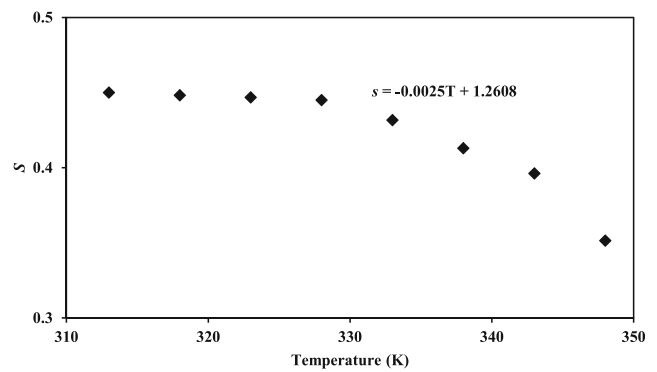**Fig. 13** ln ε_i versus ln ω at different temperatures

Fig. 14 Exponent s values versus temperature for the highest conducting electrolyte

which classified as small polaron tunnelling (SPT) [58], value of exponent s is decreased with temperature which classified as correlated barrier hopping (CBH) where the $s \rightarrow 1$ as the $T \rightarrow 0$ K [59] and lastly value of exponent s is both temperature and frequency dependent which categorized as overlapping large polaron tunnelling (OLPT) [60].

The pattern of exponent s in this work is found to decrease with temperature; hence the electrolytes in this work follow the CBH model. The differences of conduction mechanism model in electrolyte can be recognised from the value of activation energy, E_a. High activation energy prefer to tunnel though the potential barrier compared to hopping across it [61]. Kufian et al. [62] reported that PVA electrolyte doped with 33 wt.% H_3PO_4 behaved as CBH model with E_a value of 0.23 eV. Therefore, low E_a value obtained in this work showed that the ions hopping easily occur through the potential barrier which resulting on the conductivity enhancement.

Conclusion

The electrolyte system based on starch-chitosan blend doped with NH4SCN has been successfully prepared via solution-casting technique. The highest conductivity at room temperature for this system is $(1.30 \pm 0.34) \times 10^{-4}$ S cm^{-1}. The interactions between polymer blend and salt have been proven by FTIR analysis based on the shifting of hydroxyl and saccharide bands. The transport properties have been analysed using deconvolution of FTIR spectra and can be concluded that higher percentage of free ions play major part in the increment of ionic conductivity. The highest values of n, μ and D are found to be 4.01×10^{21} cm^{-3}, 2.02×10^{-7} cm^2 V^{-1} s^{-1} and 5.20×10^{-9} cm^2 s^{-1}, respectively for the highest conducting electrolyte. The deconvolution of XRD patterns has proven that S3 with 30 wt.% of salt content is the most amorphous blend with 6.98% degree of crystalinity compared to other electrolytes. The conduction mechanism in the S3 electrolyte follows the CBH model.

References

1. Fan L, Wei S, Li S, Li Q, Lu Y (2018) Recent progress of the solid-state electrolytes for high-energy metal-based batteries. Adv Energy Mater 8:1–31

2. Li Q, Chen J, Fan L, Kong X, Lu Y (2016) Progress in electrolytes for rechargeable Li-based batteries and beyond. Green energy Environment 1:18–42

3. Ramesh S, Liew CW, Arof AK (2011) Ion conducting corn starch biopolymer electrolytes doped with ionic liquid 1-butyl-3-methylimidazolium hexafluorophosphate. J Non-Cryst Solids 357:3654–3660

4. Shukur MF, Ibrahim FM, Majid NA, Ithnin R, Kadir MFZ (2013) Electrical analysis of amorphous corn starch-based polymer electrolyte membranes doped with LiI. Phys Scr 88:1–9

5. Monisha S, Mathavan T, Selvasekarapandian S, Benial AMF, Aristatil G, Mani N, Premalatha M, Pandi DV (2016) Investigation of bio polymer electrolyte based on cellulose acetate-ammonium nitrate for potential use in electrochemical devices. Carbohydr Polym 157:38–47

6. Aziz SB, Abidin ZHZ (2015) Ion-transport study in nanocomposite solid polymer electrolytes based on chitosan: electrical and dielectric analysis. J Appl Polym Sci 132:1–10

7. Nirmala Devi G, Chitra S, Selvasekarapandian S, Premalatha M, Monisha S, Saranya J (2017) Synthesis and characterization of dextrin-based polymer electrolytes for potential applications in energy storage devices. Ionics (Kiel) 23:3377–3388

8. Lin Y, Li J, Liu K, Liu Y, Liu J, Wang X (2016) Unique starch polymer electrolyte for high capacity all-solid-state lithium sulfur battery. Green Chem 18:3796–3803

9. Chatterjee B, Kulshrestha N, Gupta PN (2016) Nano composite solid polymer electrolytes based on biodegradable polymers starch and poly vinyl alcohol. Measurement 82:490–499

10. Amran NNA, Manan NSA, Kadir MFZ (2016) The effect of LiCF$_3$SO$_3$ on the complexation with potato starch-chitosan blend polymer electrolytes. Ionics 22:1647–1658

11. Khanmirzaei MH, Ramesh S, Ramesh K (2015) Polymer electrolyte based dye-sensitized solar cell with rice starch and 1-methyl-3-propylimidazolium iodide ionic liquid. Mater Des 85:833–837

12. Pokhrel S, Yadav PN, Adhikari R (2015) Applications of chitin and chitosan in industry and medical science. Sci Technol 16:99–104

13. Manigandan V, Karthik R (2018) Chitosan applications in food industry. Elsevier Inc, India, Chenai, pp 469–491

14. Zhao D, Yu S, Sun B, Gao S, Guo S, Zhao K (2018) Biomedical applications of chitosan and its derivative nanoparticles. Polymers (Basel) 10:462–479

15. Aziz SB (2018) The mixed contribution of ionic and electronic carriers to conductivity in chitosan based solid electrolytes mediated by CuNt salt. J Inorg Organomet Polym Mater 28:1942–1952

16. Aziz SB, Abdullah OG, Al-zangana S (2019) Solid polymer electrolytes based on chitosan:NH$_4$Tf modified by various amounts of TiO$_2$ filler and its electrical and dielectric characteristics. Int J Electrochem Sci 14:1909–1925

17. Kadir MFZ, Majid SR, Arof AK (2010) Plasticized chitosan-PVA blend polymer electrolyte based proton battery. Electrochim Acta 55:1475–1482

18. Muthuvinayagam M, Gopinathan C (2015) Characterization of proton conducting polymer blend electrolytes based on PVdF-PVA. Polymer (Guildf) 68:122–130

19. Mendes JF, Paschoalin RT, Carmona Alfero VB, Sena Neto R, Marques ACP, Marconcini JM, Mattoso LHC, Medeiros ES, Oliveira JE (2015) Biodegradable polymer blends based on corn-starch and thermoplastic chitosan processed by extrusion. Carbohydr Polym 137:452–458

20. Deshmukh K, Ahamed MB, Reddy A (2016) Impedance spectroscopy , ionic conductivity and dielectric studies of new Li$^+$ ion conducting polymer blend electrolytes based on biodegradable polymers for solid state battery applications. J Mater Sci Mater Electron 27:11410–11424

21. Yusof YM, Shukur MF, Illias HA, Kadir MFZ (2014) Conductivity and electrical properties of corn starch–chitosan blend biopolymer electrolyte incorporated with ammonium iodide. Phys Scr 89:1–10

22. Khiar ASA, Arof AK (2011) Electrical properties of starch/chitosan-NH$_4$NO$_3$ polymer electrolyte. Phys Math Sci 5:1662–1666

23. Hemalatha R, Alagar M, Selvasekarapandian S, Sundaresan B, Moniha V (2019) Studies of proton conducting polymer electrolyte based on PVA, amino acid proline and NH$_4$SCN. J Sci Adv Mater Devices 4:101–110

24. Nithya S, Selvasekarapandian S, Karthikeyan S (2014) AC impedance studies on proton-conducting PAN:NH$_4$SCN polymer electrolytes. Ionics (Kiel) 20:1391–1398

25. Aziz NA, Majid SR, Arof AK (2012) Synthesis and characterizations of phthaloyl chitosan-based polymer electrolytes. J Non-Cryst Solids 358:1581–1590

26. Hemalatha R, Radha KP, Rose JL (2016) AC impedance, FTIR studies of biopolymer electrolyte potato starch:NH$_4$SCN. Multidiscip Educ Res 1:4–6

27. Buraidah MH, Teo LP, Majid SR, Arof AK (2009) Ionic conductivity by correlated barrier hopping in NH$_4$I doped chitosan solid electrolyte. Phys B 404:1373–1379

28. Shukur MF, Yusof YM, Zawawi SMM, Illias HA, Kadir MFZ (2013) Conductivity and transport studies of plasticized chitosan-based proton conducting biopolymer electrolytes. Phys Scr T157:1–5

29. Hamsan MH, Shukur MF, Aziz SB, Kadir MFZ (2019) Dextran from Leuconostoc mesenteroides-doped ammonium salt-based green polymer electrolyte. Bull Mater Sci 3:42–57

30. Zulkefli FN, Navaratnam S, Ahmad AH (2015) Proton conducting biopolymer electrolytes based on starch incorporated with ammonium thiocyanate. Trans Tech 1112:275–278

31. Diederichsen KM, Buss HG, Mccloskey BD (2017) The compensation effect in the Vogel− Tammann−Fulcher (VTF) equation for polymer-based electrolytes. Macromolecules 50:3831–3840

32. Moniha V, Alagar M, Selvasekarapandian S, Sundaresan B, Boopathi G (2018) Conductive bio-polymer electrolyte iota-carrageenan with ammonium nitrate for application in electrochemical devices. J Non-Cryst Solids 481:424–434

33. Aziz SB, Faraj MG, Abdullah OG (2018) Impedance spectroscopy as a novel approach to probe the phase transition and microstructures existing in CS:PEO based blend electrolytes. Sci Rep 8:1–14

34. Aziz SB, Woo TJ, Kadir MFZ, Ahmed HM (2018) A conceptual review on polymer electrolytes and ion transport models. J Sci Adv Mater Devices 3:1–17

35. Karmakar A, Ghosh A (2014) Structure and ionic conductivity of ionic liquid embedded PEO- LiCF$_3$SO$_3$ polymer electrolyte. AIP Adv 4:1–12

36. Shukur MF, Ithnin R, Kadir MFZ (2014) Electrical properties of proton conducting solid biopolymer electrolytes based on starch–chitosan blend. Ionics (Kiel) 20:977–999

37. Tamilselvi P, Hema M (2016) Structural, thermal, vibrational and electrochemical behavior of lithium ion conducting solid polymer electrolyte based on poly (vinyl alcohol) / poly (vinylidene fluoride) blend. Poly Sci 58:776–784

38. Noor NAM, Isa MIN (2019) Investigation on transport and thermal studies of solid polymer electrolyte based on carboxymethyl

cellulose doped ammonium thiocyanate for potential application in electrochemical devices. Int J Hydrog Energy 44:1–9

39. Premalatha M, Mathavan T, Selvasekarapandian S, Mary FK, Umamaheswari R (2016) Characterization of proton conducting blend polymer electrolyte using PVA-PAN doped with NH₄SCN. Solid State Physics 1731:1–4

40. Kadir MFZ, Hamsan MH (2017) Green electrolytes based on dextran-chitosan blend and the effect of NH₄SCN as proton provider on the electrical response studies. Ionics 24:2379–2398

41. Yusof YM, Illias HA, Shukur MF, Kadir MFZ (2016) Characterization of starch-chitosan blend-based electrolyte doped with ammonium iodide for application in proton batteries. Ionics (Kiel) 23:681–697

42. Kadir MFZ, Aspanut Z, Majid SR, Arof AK (2011) FTIR studies of plasticized poly (vinyl alcohol)–chitosan blend doped with NH₄NO₃ polymer electrolyte membrane. Spectrochim Acta Part A Mol Biomol Spectroscl 78:1068–1074

43. Farghali J, Zainal B, Ahmad AH, Farghali J, Zainal B, Hanom A (2015) Conductivity study and fourier transform infrared (FTIR) characterization of methyl cellulose solid polymer electrolyte with sodium iodide conducting ion. Am Inst Phys 020026:1–5

44. Taylor P, Vicentini NM, Dupuy N, Leitzelman M, Cereda MP (2013) Prediction of cassava starch edible film properties by chemometric analysis of infrared spectra properties by chemometric analysis. Spectrosc Lett 38:749–767

45. Woo HJ, Majid SR, Arof AK (2011) Conduction and thermal properties of a proton conducting polymer electrolyte based on poly (ε - caprolactone). Solid State Ionics 199–200:14–20

46. Ramya CS, Selvasekarapandian S (2014) Spectroscopic studies on ion dynamics of PVP– NH₄SCN polymer electrolytes. Ionics:3–8

47. Rahman NAA, Navaratnam S, Abidin SS, Latif FA (2018) FTIR study on the effect of free ions in PMMA/ENR 50 polymer electrolyte system. AIP Conference 020076:1–6

48. Arya A, Sharma AL (2018) Structural, electrical properties and dielectric relaxations in Na⁺ ion conducting solid polymer electrolyte. J Phys 30:1–57

49. Ahmed HT, Abdullah OG (2020) Impedance and ionic transport properties of proton-conducting electrolytes based on polyethylene oxide/methylcellulose blend polymers. J. Sci. Adv. Mater. Devices 20:1–26

50. Arya A, Sharma AL (2019) Dielectric relaxations and transport properties parameter analysis of novel blended solid polymer electrolyte for sodium-ion rechargeable batteries. J Mater Sci 54:7131–7155

51. Ramlli MA, Ikmar M, Mohamad N (2016) Structural and ionic transport properties of protonic conducting solid biopolymer electrolytes based on carboxymethyl cellulose doped ammonium fluoride. J Phys Chem B 120:11567–11573

52. N. H. Muhamaruesa, M. Ikmar (2017) Studies of ionic conductivity and A.C. conduction mechanism of 2-hydroxyethyl cellulose based solid polymer electrolytes. Sustain. Sci. Manag. 65–70

53. Selvalakshmi S, Vijaya N, Selvasekarapandian S, Premalatha M (2017) Biopolymer agar-agar doped with NH₄SCN as solid polymer electrolyte for electrochemical cell application. Appl Polym Sci 44702:1–10

54. Adnan SBRS, Mohamed NS (2014) Electrical properties of novel Li₄.₀₈Zn₀.₀₄Si₀.₉₆O₄ ceramic electrolyte at high temperatures. Ionics (Kiel) 20:1641–1650

55. Iqbal MZ, Rafiuddin (2015) Structural, electrical conductivity and dielectric behavior of Na₂SO₄- LDT composite solid electrolyte. J Adv Res 7:135–141

56. Chandra A (2013) Synthesis and dielectric studies of PEO-PVP blended solid polymer electrolytes. Pure Appl Phys 51:788–791

57. Ben Gzaiel M, Oueslati A, Hlel F, Gargouri M (2016) Synthesis, crystal structure, phase transition and electrical conduction mechanism of the new [(C₃H₇)₄N]₂MnCl₄ compound. Phys E Low-dimensional Syst Nanostructures 85:405–413

58. Rahmouni H, Smarib M, Cherifa B, Dhahrib E, Khirounia K (2015) Conduction mechanism, impedance spectroscopic investigation and dielectric behavior of La₀.₅Ca₀.₅₋ₓAgₓMnO₃ manganites with the composition below the concentration limit of silver solubility in perovskites (0≤x≤0.2). Dalt Trans 44:10457–10466

59. Ajili O, Louati B, Guidara K (2018) Electrical properties and conduction mechanism by CBH model of Na₂SrP₂O₇. J Mater Sci Mater Electron 29:8649–8659

60. Chakchouk N, Louati B, Guidara K (2018) Electrical properties and conduction mechanism study by OLPT model of NaZnPO₄ compound. Mater Res Bull 99:52–60

61. Nasri S, Megdiche M, Gargouri M (2014) Electrical conduction and dielectric properties of a newly synthesized single phase:Ag₀.₄-Na₀.₆FeP₂O₇. Phys B Phys Condens Matter 451:120–127

62. Kufian MZ, Majid SR, Arof AK (2007) Dielectric and conduction mechanism studies of PVA- orthophosphoric acid polymer electrolyte. Ionics (Kiel) 13:231–234